Physica D 333 (2016) 235–242

Contents lists available at ScienceDirect

Physica D

journal homepage: www.elsevier.com/locate/physd

Self-focusing dynamics of patches of ripples

P.A. Milewski [a], Z. Wang [b,a,*]

[a] Department of Mathematical Sciences, University of Bath, Bath BA2 7AY, UK

[b] Key Laboratory for Mechanics in Fluid Solid Coupling Systems, Institute of Mechanics, Chinese Academy of Sciences, Beijing 100190, China

HIGHLIGHTS

- High resolution computations of capillary gravity wave packets from primitive fluid equations.
- Primitive dynamics of packets compared to solutions of critical, focussing, 2D NLS.
- Similarities and contrasts with focussing of light beams in Kerr media discussed.
- Long time dynamics – beyond validity of NLS – explored.

ARTICLE INFO

Article history:
Received 2 September 2015
Available online 23 March 2016

Keywords:
Ripples
Focussing
Wavepackets

ABSTRACT

The dynamics of focussing of extended patches of nonlinear capillary–gravity waves within the primitive fluid dynamic equations is presented. It is found that, when the envelope has certain properties, the patch focusses initially in accordance to predictions from nonlinear Schrödinger equation, and focussing can concentrate energy to the vicinity of a point or a curve on the fluid surface. After initial focussing, other effects dominate and the patch breaks up into a complex set of localised structures – lumps and breathers – plus dispersive radiation. We perform simulations both in the inviscid regime and for small viscosities. Lastly we discuss throughout the similarities and differences between the dynamics of ripple patches and self-focussing light beams.

1. Introduction

The nonlinear Schrödinger equation (NLS) is a universal model that appears in many contexts in science, including nonlinear optics, plasma physics, and hydrodynamics [1] and provides a canonical description for the evolution of the envelope of dispersive and/or diffracting quasi-monochromatic, plane, weakly nonlinear waves. The envelope of free-surface water-wave packets can thus be approximated by $2+1$ dimensional cubic NLS equation in the small-amplitude deep-water limit [2]. For capillary–gravity (CG) waves, that is, when the effects due to gravity and surface tension are equally important, the associated NLS equation is of the *focusing* type [3,2]. This equation has solutions which, under certain conditions, become singular in finite time [4]. The natural question we address in this paper is to what extent the focussing collapse behaviour, whereby the energy of the wavepacket is focussed to the neighbourhood of a point or a curve, can be observed in the *full* surface wave equations (confirming the NLS prediction) when appropriate initial conditions are given. Furthermore, one would also like to find out what physical effects, if any, arrest the focussing, and the dynamical behaviour that ensues after the focussing time.

Nonlinear capillary–gravity are of intrinsic interest due to their complexity and play an important role in atmosphere–ocean coupling (see e.g. [5]). In contrast to the KdV soliton which occurs in two-dimensional shallow water and is localised only in the propagation direction, fully localised CG solitary waves ("lumps") can be found on the surface of a three-dimensional fluid of arbitrary depth [6]. In very shallow water (characterised by a Bond number $\sigma/\rho g d^2$ larger than $1/3$ corresponding to a depth d of a few millimetres in water), these lumps bifurcate from zero wavenumber and can be approximated by solutions of the Kadomtsev–Petviashvili (KPI) equation [7]. This regime is physically less realistic in view of the additional dissipation due to bottom friction. In a more realistic, deeper water regime (when the Bond number is less than 1/3—see Table 1 for physical parameters) these lumps bifurcate from the minimum of the dispersive phase-speed occurring at finite wavenumber [3,8,6]. Therefore, small-amplitude lumps in deep water can be approximately constructed

* Corresponding author at: Key Laboratory for Mechanics in Fluid Solid Coupling Systems, Institute of Mechanics, Chinese Academy of Sciences, Beijing 100190, China.
E-mail address: zwang@imech.ac.cn (Z. Wang).

http://dx.doi.org/10.1016/j.physd.2016.03.010

Table 1
Physical parameters for water and mercury.

Parameter	Symbol	Water	Mercury
Fluid density	ρ (kg/m^3)	998	13 579
Surface tension	σ (N/m)	0.0728	0.48
Kinematic viscosity	ν (m^2/s)	1.307×10^{-6}	0.114×10^{-6}
Reynolds number	Re	341	2270
CG wavelength ($k = 1$)	λ (cm)	1.7	1.2
CG phase speed ($k = 1$)	c_p (cm/s)	16.1	13.6
Deep water regime	(cm)	>0.9	>0.6

by using the localised ground state of the focussing NLS (called the Townes profile [9]) to modulate a carrier wave with minimum phase speed [3,10], and occur in a variety of models where they also coexist with unstable elevation waves [3,11]. These small-amplitude lumps are known to be unstable, which can be seen by either recalling that the Townes Profile is unstable within the focussing NLS or by direct computation on the full equations. However, certain larger-amplitude lumps occurring on the same branch of solution beyond the regime of validity of NLS have been constructed numerically, and are stable [6,10]. In addition, these lumps coexist with stable breathers which appear in time dependent computations. These lumps and breathers seem to act as "attractors" for the dynamics of the inviscid CG waves whenever wavepackets constructed from a perturbed TP or from higher energy states of NLS evolve in time [10]. The stable structures will play an important part in the evolution of more general collapsing wavepackets considered here, particularly in arresting the focussing dynamics.

Deep water lumps have recently been observed in laboratory experiments with water, where they are excited by a moving jet of air, directed at the surface, at a constant subcritical speed. The lumps are generated behind the jet where free depression lumps are shed, but then quickly dissipate due to the viscous effect [12]. Simulations of a similar mechanism – albeit in shallow water – was discussed in [13].

In this paper we report the results of "numerical wavetank" experiments in the modulated CG wave regime. Direct time-dependent numerical simulations of surface waves in the primitive Euler equations with a variety of initial data consisting of modulated CG waves (Gaussian, super-Gaussian etc.) are performed. The computations are achieved with a truncated Hamiltonian formulation of potential flow, and, in some cases, include a small-viscosity limit model [10]. Our results confirm the self-focussing predictions of the cubic NLS, and show an eventual breakdown of the focussing structures into a complex set of localised lumps and breathers, together with some dispersive radiation. The transition between an NLS-like focussing behaviour and the emergence of lumps and breathers occurs when the modulation lengthscale has focussed to be comparable to the carrier wavelength. The phenomena computed here should be observable in laboratory wave experiments using mercury [14], or water in microgravity, as these conditions would reduce the relative effect of viscosity (see Table 1).

The universality of the NLS equation and its centrality in nonlinear optics has led recently to many water-wave-nonlinear optics analogies, primarily between *gravity* waves on the surface of a *two dimensional* fluid domain, such as undular bores, the Peregrine soliton, etc. and light propagation in optical fibres (see, for example, [15,16] and references therein). In a similar spirit we also discuss analogies and contrasts between three-dimensional capillary–gravity water waves and light beams in Kerr media. The simplest fundamental model for a light beam propagating in a bulk medium is the $2+1$ dimensional focusing cubic NLS. The collapse dynamics occurs when the initial beam power is above a critical value and the nonlinear Kerr effect due to the intensity-dependent refractive index overcomes linear diffraction, self-focussing the beam to extreme intensities. The lowest collapse power is achieved by the Townes profile (TP) [9] which was discovered in this context. Experiments in [17] show that a collapsing Gaussian beam can evolve to the TP singularity, but recent theoretical [18] and experimental [19] studies show that if the initial beam has a sharper intensity modulation (e.g. a "super-Gaussian" profile in the plane transverse to beam propagation) and sufficiently strong power, the dynamical behaviour is distinct from the Gaussian beam, and the beam evolves towards a self-similar high-intensity collapse on a ring. Eventually, a variety of large amplitude effects (dependent on initial power) will halt the collapse [20]. In [21] the primitive Maxwell equations are solved in a model for light propagation in a bulk dielectric and some features of optical self focussing are observed.

In all water-wave-nonlinear optics analogies, one must keep in mind that while NLS is an extremely accurate model in optics, its range of applicability in water waves is more restricted—in particular by the limited range of amplitudes and modulation scales that are physically achievable.

2. Formulation

The equations for the surface elevation $\eta(\mathbf{x}, t)$ and the inviscid velocity potential $\xi(\mathbf{x}, t)$ at the surface for a weakly viscous incompressible flow (as modelled in [22]) is described by [10]

$$\eta_t - G_0\xi = 2\mathrm{Re}^{-1}\Delta\eta + (G_1 + G_2)\,\xi, \tag{1}$$

$$\begin{aligned}\xi_t + (1-\Delta)\,\eta = {} & 2\mathrm{Re}^{-1}\Delta\xi + \frac{1}{2}\Big[(G_0\xi)^2 - |\nabla\xi|^2 \\ & + 2\,(G_0\xi)\,(G_1\xi + \nabla\xi\cdot\nabla\eta)\Big] \\ & + \nabla\cdot\left[\frac{\nabla\eta}{\sqrt{1+|\nabla\eta|^2}} - \nabla\eta\right]\end{aligned} \tag{2}$$

with

$$G_0 = (-\Delta)^{1/2}, \qquad G_1 = \nabla\cdot\eta\nabla - G_0\eta G_0,$$
$$G_2 = \frac{1}{2}\left(G_0\eta^2\Delta + \Delta\eta^2 G_0 + 2G_0\eta G_0\eta G_0\right).$$

The system (1)–(2) is non-dimensional, with the fluid density ρ, the gravitational acceleration g and the surface tension coefficient σ of the fluid, having been removed by proper rescaling (see [10]). The dimensional spatial and temporal scales for some fluids are given in Table 1. The only parameter remaining in the problem is the Reynolds number Re defined as

$$\mathrm{Re} = \frac{\text{inertial forces}}{\text{viscous forces}} = \frac{1}{\nu}\left(\frac{\sigma^3}{\rho^3 g}\right)^{1/4}$$

where ν is the kinematic viscosity of the fluid. In the inviscid limit ($\mathrm{Re}\to\infty$), the system (1)–(2) has Hamiltonian structure, with canonical variables ξ and η, and Hamiltonian given by

$$\begin{aligned}\mathcal{H}[\eta,\xi] = \frac{1}{2}\int_{\mathbb{R}^2}\Big[\xi\,(G_0 + G_1 + G_2)\,\xi + \eta^2 \\ + 2\left(\sqrt{1+|\nabla\eta|^2} - 1\right)\Big]\,dxdy.\end{aligned} \tag{3}$$

In the modulational regime, the envelope of quasi-monochromatic inviscid CG waves are governed by the cubic NLS. Taking a modulated sinusoid solution with wave number $\mathbf{k} = (k, l)$ and frequency ω, where $\omega^2 = |\mathbf{k}|\left(1 + |\mathbf{k}|^2\right)$

$$\eta = \epsilon\tilde{A}(\tilde{X},\tilde{Y},\tau)e^{i(kx+ly-\omega t)} + \text{c.c.} + O(\epsilon^2), \tag{4}$$

$$\xi = \epsilon\tilde{B}(\tilde{X},\tilde{Y},\tau)e^{i(kx+ly-\omega t)} + \text{c.c.} + O(\epsilon^2), \tag{5}$$

standard asymptotic methods applied to the system (1)–(2) yields,

$$i\tilde{A}_\tau + \lambda_1 \tilde{A}_{\tilde{X}\tilde{X}} + \lambda_2 \tilde{A}_{\tilde{Y}\tilde{Y}} + \gamma |\tilde{A}|^2 \tilde{A} = 0, \tag{6}$$

with $\tilde{B} = -i\frac{\omega}{|k|}\tilde{A}$ and where ϵ is a small parameter governing the amplitude and modulation scales $(\tilde{X}, \tilde{Y}, \tau) = \left(\epsilon(x - c_g t), \epsilon y, \epsilon^2 t\right)$, where $c_g = \omega_k$ is the group velocity. Assuming, without loss of generality, that the carrier wave propagates in the x direction (i.e. $l = 0$), the NLS coefficients are given by

$$\lambda_1 = \frac{\omega_{kk}}{2}, \qquad \lambda_2 = \frac{\omega_k}{2k}, \qquad \gamma = \frac{\omega k^2}{4}\frac{2k^4 + k^2 + 8}{(2k^2 - 1)(1 + k^4)}. \tag{7}$$

A fundamental difference between derivation the cubic NLS in water wave problems and in optical beams arises from the geometry of the problem. In nonlinear optics, the modulation is in the plane perpendicular to the propagation direction (i.e. transverse to the beam) so that the linear dispersive terms in NLS, arising from the parabolic approximation to the wave equation, are isotropic ($\lambda_1 = \lambda_2 > 0$). In water wave problems, the modulation is both in the direction of propagation and transverse to it, and the effects leading to the dispersive terms are distinct. $\lambda_2 > 0$ arises, as in nonlinear optics, from transverse modulations (the curvature of wavefronts), whereas λ_1 arises from usual dispersive effects in the propagation direction and may be of either sign. In optics, the Kerr nonlinearity is material dependent and results in $\gamma > 0$ in most materials (a decrease in wavespeed with amplitude), whereas in water waves, the Stokes' nonlinear correction to wave speed may lead to either sign for γ. From the above relations (7), it is clear that for the water wave capillary or the capillary gravity regime, when $k > \frac{1}{\sqrt{2}}$, then $\lambda_1 > 0$ (shorter waves travel faster), $\lambda_2 > 0$ and $\gamma > 0$ (larger waves travel more slowly). Then, the equation is of the same type as the focusing cubic NLS arising in nonlinear optics. One quantitative difference, however, is that since $\lambda_1 \neq \lambda_2$, focussing is not isotropic, and a uniformly focussing patch of ripples will have an envelope with transverse-to-propagation lengthscale ratio $\sqrt{\lambda_2/\lambda_1}$. Finally, in water waves, the wavenumber $k = 1$ is particularly important as, at this wavelength, the group and phase speeds of dispersive surface waves are equal, and therefore localised wave packets are *steadily* travelling solitary waves. This is the regime where lumps can be found. For the remainder of the paper we shall restrict ourselves to this regime although similar focussing dynamics occurs over a range of wavenumbers near $k = 1$. For $k = 1$ we have

$$\lambda_1 = \frac{\sqrt{2}}{4}, \qquad \lambda_2 = \frac{\sqrt{2}}{2}, \qquad \gamma = \frac{11\sqrt{2}}{8}.$$

Since the signs of the coefficients are positive, one can normalise NLS (6) with $\tilde{X} = X/\sqrt{\lambda_1}$, $\tilde{Y} = Y/\sqrt{\lambda_2}$ and $\tilde{A} = A/\sqrt{\gamma}$ such that one obtains a new equation for $A(X, Y, \tau)$ with $\lambda_1 = \lambda_2 = \gamma = 1$. The solution of this equation then conserves mass

$$\mathcal{M} = \int |A|^2 \, dXdY,$$

and its Hamiltonian energy

$$\mathcal{E} = \int (|\nabla A|^2 - \frac{1}{2}|A|^4) \, dXdY.$$

A virial argument (see [4]) shows that, the variance

$$\mathcal{V} = \int (X^2 + Y^2)|A|^2 \, dXdY$$

satisfies $\mathcal{V}'' = 8\mathcal{E}$. Therefore, if $\mathcal{E}$ is initially negative, the solution will focus and blowup in finite time as $\mathcal{V} \to 0$—the so-called wave collapse. Dissipation from (1)–(2) leads to a linear damping term in NLS, but this does not arrest blowup in general – that is – for any given fixed damping parameter there exists initial data that blows up in finite time [23–25]. For $\mathcal{E}$ positive, $\mathcal{V}$ increases without bound corresponding to the dispersive spreading of the wave. The Townes profile can be obtained as the minimiser for $\mathcal{M}$ with $\mathcal{E} = 0$ and therefore corresponds to the unstable boundary state between blowup and spreading solutions. This argument applies only to NLS. It does not rule out stable solitary wave solutions to the original CG water wave problem (1)–(2) at larger amplitudes. Such solutions in fact exist: they are the lumps found in [10,6] (see Fig. 1) and will play a role in the dynamics shown below.

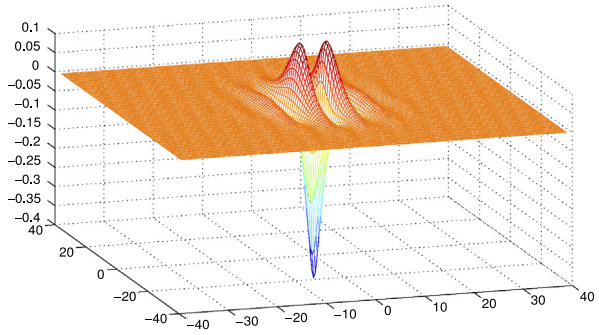

Fig. 1. Stable solitary CG wave ("lump"). Breathers have similar profile with time periodic amplitude oscillations.

3. Numerical simulations

Using a pseudo-spectral method, we simulate the dynamical equations (1)–(2) in a spatially double-periodic domain on a grid consisting of 256 × 512 or 256 × 1024 nodes in transverse and wave propagation directions respectively. Time integration of the system is accomplished with a Runge–Kutta method combined with an integrating factor (the detailed description of the numerical method and code validation can be found in [10]). All the computations are de-aliased with a doubling of Fourier modes. The Hamiltonian expression (3) is a conserved quantity in the inviscid case and is used to check the global accuracy of our numerical computations.

In all computations, we initialise (1)–(2) with a packet modulated by an envelope $A_0(X, Y)$ (see (4)–(5)):

$$\eta(x, y, 0) = 2\epsilon \frac{1}{\sqrt{\gamma}} A_0\left(\frac{\epsilon x}{\sqrt{\lambda_1}}, \frac{\epsilon y}{\sqrt{\lambda_2}}\right) \cos(kx) \tag{8}$$

$$\xi(x, y, 0) = 2\epsilon \frac{\omega}{k}\frac{1}{\sqrt{\gamma}} A_0\left(\frac{\epsilon x}{\sqrt{\lambda_1}}, \frac{\epsilon y}{\sqrt{\lambda_2}}\right) \sin(kx). \tag{9}$$

The envelope A_0 is taken as one of the following

$$A_g, A_{sg}, A_{sq} = \alpha\, e^{-\frac{(X^2+Y^2)}{\beta}}, \alpha\, e^{-\frac{(X^2+Y^2)^2}{\beta^2}}, \alpha\, e^{-\frac{(X^4+Y^4)}{\beta^2}},$$

where the subscripts stand for Gaussian, super-Gaussian and square, respectively. It follows that

$$\mathcal{M}_g = \pi\alpha^2\beta/2, \qquad \mathcal{M}_{sg} = \pi^{3/2}\alpha^2\beta/2\sqrt{2},$$
$$\mathcal{E}_g = \pi\alpha^2\left(1 - \alpha^2\beta/8\right), \qquad \mathcal{E}_{sg} = 2\pi\alpha^2\left(1 - \alpha^2\beta\sqrt{\pi}/16\right),$$
$$\mathcal{V}_g = \mathcal{V}_{sg} = \pi\alpha^2\beta^2/4.$$

To obtain focusing of the wavepacket, we choose α and β such that $\mathcal{E}$ is negative which requires $\mathcal{M}$ to be sufficiently large. In the water wave problem $\mathcal{M}$ is proportional to the leading order Hamiltonian energy of the waves

$$\mathcal{H} \approx (1 + k^2)\int |\tilde{A}|^2 \, d\tilde{X}d\tilde{Y} = \frac{(1 + k^2)}{\gamma}\mathcal{M} \approx 1.03\mathcal{M},$$

where we have taken $k = 1$ in the last step.

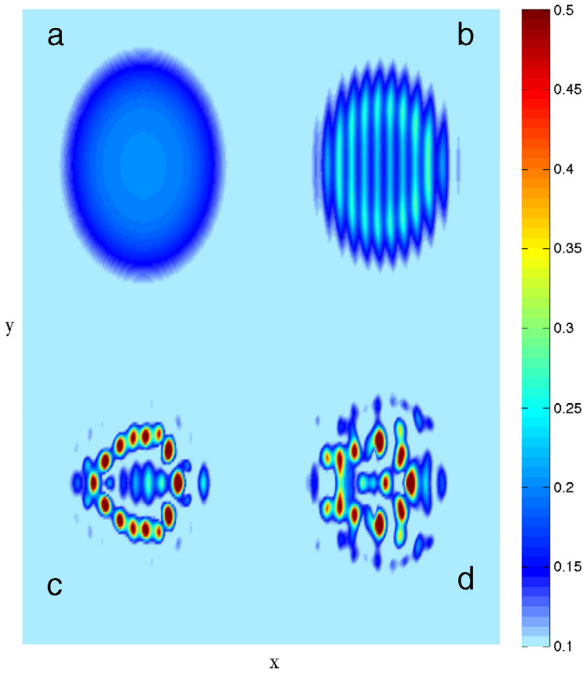

Fig. 2. Evolution of the wave envelope function $\mathbb{E}$ extracted from solutions to (1)–(2) with an initial super-Gaussian profile in (8)–(9). For this data $\mathcal{H} = 238.7 \approx 1.03\mathcal{M} = 238.5$. The images are taken at (a) $t = 0$ (b) $t = 125$ (c) $t = 200$ (d) $t = 250$. The NLS collapse time is ≈ 306. (For interpretation of the references to colour in this figure legend, the reader is referred to the web version of this article.)

In optics $\mathcal{M}$ is the power of the beam and in collapse experiments is usually measured in multiples of the Townes' profile power $\mathcal{M}_T$ which is approximately 11.7 in this scaling. In the water wave setting, the minimum energy of a finite amplitude *stable* lump – which is not captured by NLS – is $\mathcal{H} \approx 6.1$. As was shown in [10], a collapsing perturbed Townes profile with $\mathcal{H} \approx 12.1$, after radiating some energy, generates a lump or breather with $12.1 > \mathcal{H} > 6.1$.

The wave collapse time for Gaussian and super-Gaussian can be respectively found as

$$\tau_g^* = \sqrt{\frac{\beta^2}{2(\alpha^2\beta - 8)}}, \quad \text{for } \alpha^2\beta > 8, \tag{10}$$

$$\tau_{sg}^* = \sqrt{\frac{\beta^2}{2(\sqrt{\pi}\alpha^2\beta - 16)}}, \quad \text{for } \alpha^2\beta > \frac{16}{\sqrt{\pi}}. \tag{11}$$

This result applies to the collapse to a point and only gives an upper bound to the time for other types of collapse.

If fluid experiments were performed to observe these phenomena, one would replace the use of an initial condition (8)–(9) with a wavemaker capable of producing a modulated packet. That is, the paddles would oscillate at the carrier frequency and their amplitudes would be modulated both in space and in time to produce an emerging patch of ripples of the form (8).

We have chosen parameters for the numerical experiments that would be physically feasible in a laboratory. The energy $\mathcal{H}$ of the wavepacket is independent of ϵ, but the size of the packet and its focussing time are not. In particular for $k = 1$, $\sqrt{\beta\lambda_1}/\pi\epsilon$ is the number of carrier wavelengths in the packet, which is chosen here to be in the range 12–25. The distance travelled by the packet in the time for collapse, for sufficiently large energy, is approximately $\sqrt{\beta}/2\pi^{5/4}\alpha\epsilon^2$ in units of wavelengths. This is chosen to be in the range 60–250, although we shall see that the wavepacket breaks down before the collapse time. This regime corresponds to $\mathcal{M} \approx 20\mathcal{M}_T$, which is a regime for which, within

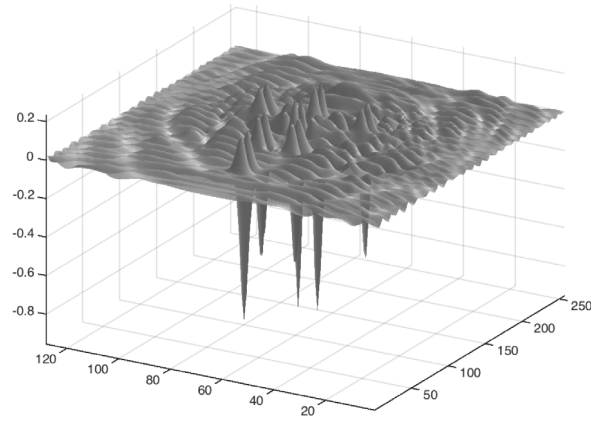

Fig. 3. Closeup of a typical free-surface for a focussing super-Gaussian patch at late times.

NLS, Gaussian profiles collapse to a point, but super-Gaussian profiles collapse to a ring [19]. The regime also gives an upper bound on the number of stable localised structures that can be generated. Physical experimental dimensions corresponding to this regime can then be concluded from Table 1.

Once solutions to (1)–(2) are obtained, an approximation to the wave envelope is defined by

$$\mathbb{E} = \sqrt{\eta^2 + |\mathcal{R}[\eta]|^2}. \tag{12}$$

Here, $\mathcal{R}$ is the Riesz transform, which can be defined as a Fourier multiplier, namely

$$\widehat{\mathcal{R}[\eta]}(k,l) = \left(\frac{ik}{\sqrt{k^2+l^2}}, \frac{il}{\sqrt{k^2+l^2}}\right)^\top \widehat{\eta}(k,l),$$

where $\widehat{\cdot}$ represents the Fourier transform. This is a natural way to identify the wavepacket in the modulational regime, from (4). This expression has been proposed in [26], in the one-dimensional case, where the Riesz transform is replaced by the Hilbert transform which shifts a sinusoid by half its period and hence, when combined as above, removes the fast oscillation from a modulated signal.

We will compare the solutions obtained from direct computation on the fluid equations to those of NLS. At typical amplitudes, nonlinear water waves have a prominent second harmonic component (the $\epsilon^2 e^{2i(x-\omega t)}$ terms in (4)–(5)), and therefore it is useful to understand how $\mathbb{E}$ depends on higher order terms. After solving these terms using the full equations, restricting to $k = 1$, and substituting (4) in $\mathbb{E}$ one obtains

$$\mathbb{E} = 2\epsilon|\tilde{A}|\left[1 - \epsilon(\tilde{A}e^{ix} + \tilde{A}^* e^{-ix}) + O(\epsilon^2)\right]. \tag{13}$$

The first experiment, presented in Fig. 2, shows snapshots of the time evolution of $\mathbb{E}$ for a focussing CG wave packet computed from the inviscid limits of (1)–(2) (ie $Re = \infty$), with initial super-Gaussian modulation envelope (time increases in the four frames from top-left to bottom-right). The parameters chosen were $\epsilon = 0.1$, $\alpha = -1.4$ and $\beta = 60$ and the figures are in a frame of reference moving with the patch. In this experiment, as elsewhere in the paper, the scales of the x and y axes are chosen to be equal. In the time sequence we see a smooth envelope generating nonlinearly a second harmonic (the vertical stripes in the second panel) with an amplitude increase on an ellipse. This is followed by a continued focussing of energy in which the focussed region breaks up into a large number of high intensity spots. These are depression lumps and/or breathers that appear as the red spots in third and fourth panels. The onset of breakup into these structures can be approximately predicted using their

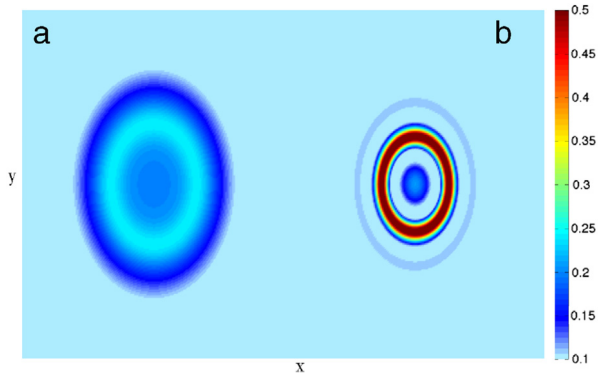

Fig. 4. Evolution of $|A|$ in NLS equation for the same initial data as in Fig. 2 at the two intermediate times: (a) $t = 125$ (b) $t = 200$.

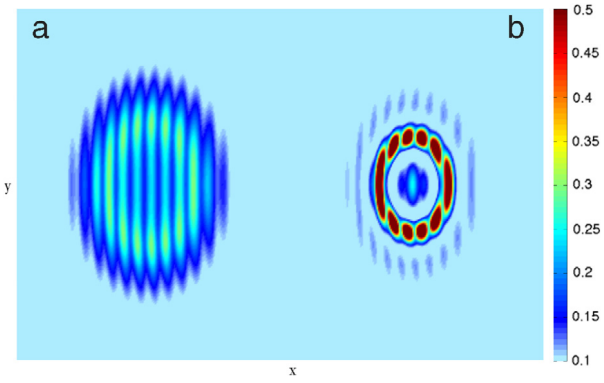

Fig. 5. Evolution of $\mathbb{E}$ reconstructed from the NLS equation for the same initial data as in Fig. 2 at the two intermediate times: (a) $t = 125$ (b) $t = 200$. These images should be compared to Fig. 2(b) and (c).

characteristics from [10]: the *stable* lumps exist for $c < c^* \approx 1.404$, where c^* is the speed at which they attain their energy minimum on the branch of solutions. From the NLS equation, the speed–amplitude dependence of the carrier wave is $c = \sqrt{2} - \gamma\epsilon^2|\tilde{A}|^2$. Thus, stable lumps can be generated when $|\epsilon\tilde{A}|$ is larger than $0.1/\sqrt{\gamma}$. Each of these spots is a localised structure similar to the one shown in Fig. 1. In Fig. 3 we show a typical free surface image where a number of these waves are apparent. These lumps and breathers continue to interact and merge in a complex manner – their collisions are inelastic (see [10]) – and the initial coherence of the modulation is completely lost (fourth panel). These computations further strengthen observations in [10] that lump and breather structures appear naturally as "attractors" of CG inviscid nonlinear water wave dynamics. In Figs. 4 and 5 are shown computations based on the NLS equation for the same initial data. Fig. 4 shows the modulation amplitude $|A|$ at the two intermediate times of Fig. 2, showing the clear focussing on an ellipse. Fig. 5 shows the same data at the same times but adding a second harmonic component consistent with the modulation expansion of the free surface equations (see (13)) so that the solutions can be compared directly with Fig. 2. In Fig. 6 we show the Fourier spectrum of the solution presented in Fig. 2. One sees clearly the generation of the second harmonic followed by, in the third panel, a broadband spectrum indicating the solution in no longer well approximated by the NLS equation.

The next set of figures depicts three numerical experiments with different initial envelopes. The first one shown in Fig. 7 uses the "square" initial data: the largest initial gradient of the envelope $|A|$ lies in the neighbourhood of a square in the plane. The evolution shows that the focussing occurs on a similar curve (see [19] for an argument based on the high power limit). The following two figures highlight the fact that the water wave problem in this regime is not invariant under rotations of the carrier wavevector, an effect which does not arise in the optical beam case. In particular we take an envelope that is Gaussian in one variable and Super-Gaussian in the other. In Fig. 8 the envelope is given by $A_0 = \alpha \exp(X^4/\beta^2) \exp(Y^2/\beta)$ and thus the initial focussing is expected to be the largest at the front and back of the packet (see the third and fourth panels in Fig. 8) in fact splitting the packet. In Fig. 9 the variables X and Y are exchanged (corresponding to a $\pi/2$ rotation of the wavevector) and the behaviour is markedly different, particularly after initial focussing. Note that the different aspect ratio in the two experiments arises from the scaling required by the non-isotropic nature of the diffraction in the surface wave NLS.

A second set of experiments were performed including dissipation in the water wave equations. The computations were made using $\mathrm{Re} = 2272$ in (1)–(2), as a model for CG waves on

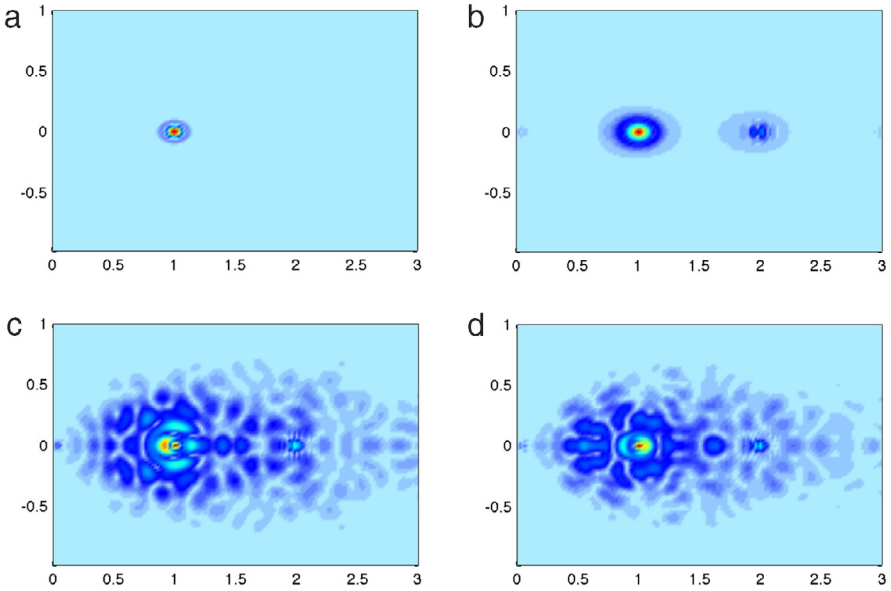

Fig. 6. Fourier spectral amplitude of solutions to (1)–(2) for the same initial data as in Fig. 2 at (a) $t = 0$ (b) $t = 125$ (c) $t = 200$ (d) $t = 250$. Only the $k \geq 0$ part of the spectrum is shown.

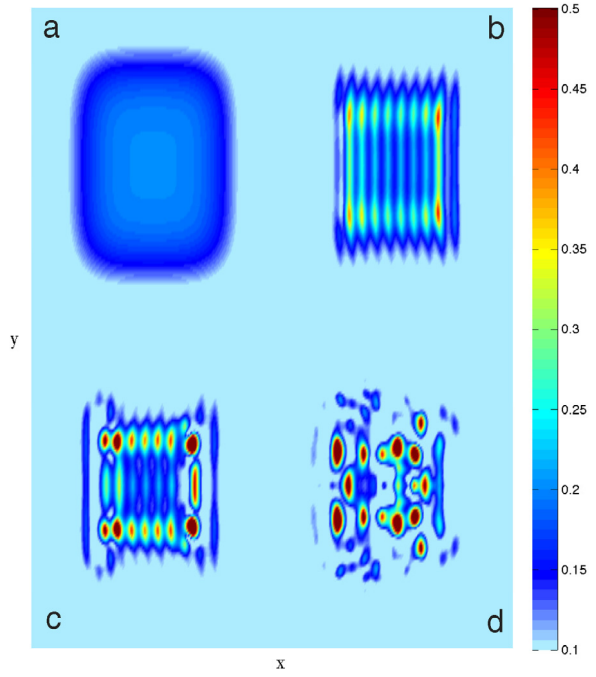

Fig. 7. Evolution of $\mathbb{E}$ for an initially "square" envelope profile. The parameters were chosen as follows: $\epsilon = 0.1$, $\alpha = -1.4$, $\beta = 60$. The images are at (a) $t = 0$ (b) $t = 160$ (c) $t = 200$ (d) $t = 300$.

the surface of mercury (see Table 1). Given that the spectrum has $k \geq 1$, the viscous decay time in (1)–(2) is less than 0.5Re and the focussing phenomena may be observed if the collapse time is comparable. Figs. 10 and 11 show the focussing of a Gaussian modulation packet in two cases, where the only difference is π in the relative phase of the carrier wave with respect to the modulation. In Fig. 10 the trough of the surface wave is at the centre of the packet, whereas in Fig. 11 the crest is at the centre. The NLS equation does not distinguish between these two cases. Nonlinear surface waves, however, have a strong asymmetry between crests and troughs, and the two computations eventually differ during the focussing evolution, the depression wave having a faster evolution. The parameters chosen for this experiment are $k = 1$, $\epsilon = 0.1$, $\alpha = -1.736$ and $\beta = 60$.

In Fig. 12 a super-Gaussian packet of the same initial water wave energy as in the inviscid case of Fig. 2 is shown evolving in the dissipative system. The experiment confirms that ring focussing can be observed despite the presence of damping, although there is substantial decay in the energy.

We conducted further experiments varying the carrier wavenumber k within the range $0.75 \leq k \leq 1.25$. Recall that for smaller wavenumbers the NLS ceases to focus and for larger wavenumbers dissipation would prevent physically observable phenomena. At lower k the dynamics includes even stronger second harmonic generation due to the resonance corresponding to Wilton ripples at $k = \sqrt{2}/2$. In these cases a secondary disturbance propagates ahead of the patch and may create a second focussing region. Larger k packets also focus, but the evolution is characterised by a frequency downshift before the generation of lumps, which have most of their energy near $k = 1$.

4. Conclusions

In physically realistic situations, the strong focussing of capillary–gravity wavepackets can occur, with, as a consequence, the generation of fully localised structures such as lumps and breathers. The initial stages of this focussing is well captured by

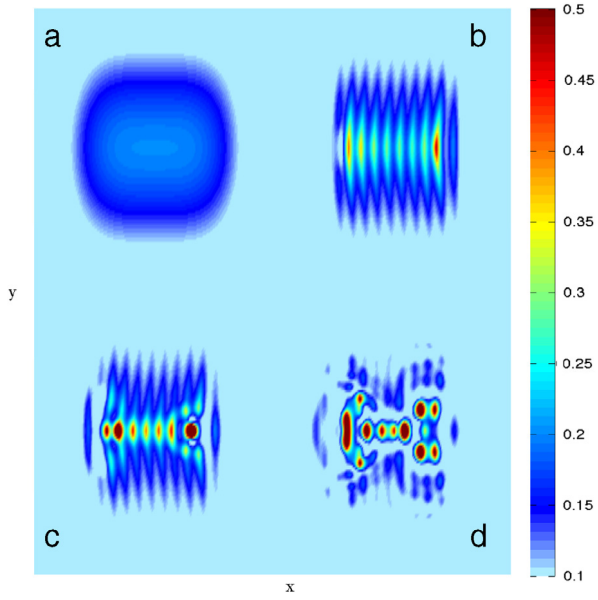

Fig. 8. Evolution of $\mathbb{E}$ for a wavepacket with super-Gaussian variation in x and Gaussian in y. The parameters are $\epsilon = 0.1$, $\alpha = -1.4$ and $\beta = 60$. The images are shown for (a) $t = 0$ (b) $t = 160$ (c) $t = 200$ (d) $t = 250$.

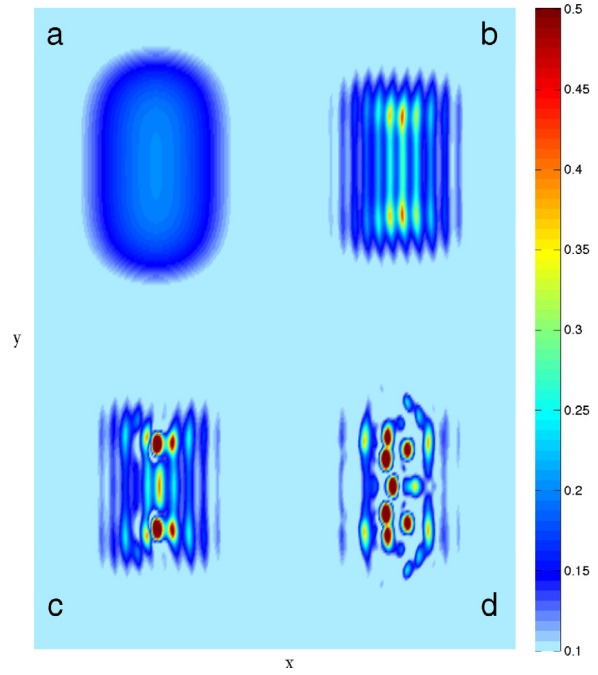

Fig. 9. Evolution of $\mathbb{E}$ for a wavepacket with super-Gaussian variation in y and Gaussian in x with the same parameters as in Fig. 8. The images are shown for (a) $t = 0$ (b) $t = 160$ (c) $t = 200$ (d) $t = 250$.

the NLS equation and therefore there are similarities with the self-focussing of light beams. In particular, at large energies (compared to the ground state of the NLS equation) one can obtain focussing in the vicinity of curves on the surface (ellipses, rectangles). In the water wave case, however, the NLS regime is fairly short lived for realisable situations: in the experiments we have conducted NLS focussing results in an amplification of the surface wave by a factor of 2–3, after which the wavepacket breaks up into localised structures which undergo complex dynamical interactions. By contrast, NLS is a very accurate model for light, and experiments where focussing is observed over a greater range of amplitudes,

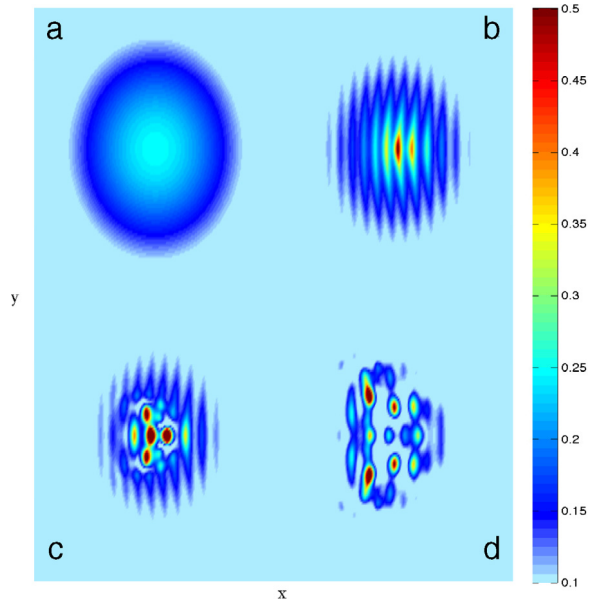

Fig. 10. Viscous evolution of the wave envelope $\mathbb{E}$ extracted from (1)–(2) with an initial Gaussian profile in (9)–(10). The images are taken at (a) $t = 0$ (b) $t = 152$ (c) $t = 200$ (d) $t = 300$. We chose parameters $\epsilon = 0.1$, $\alpha = -1.736$ and $\beta = 60$. For this data $\mathcal{H} = 292.8 \approx 1.03\mathcal{M} = 292.6$. The NLS collapse time is approximately 323.

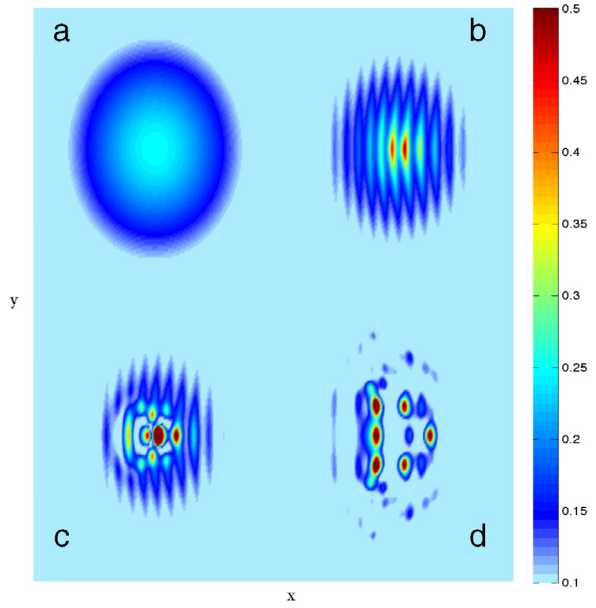

Fig. 11. Similar experiment to that in Fig. 10, except that the carrier wave shifted by π (i.e. $\alpha = 1.736$).

have been performed. Due to the short lived nature of the focussing NLS regime in water waves, some of the phenomena observed in optics, such as the azimuthal instability of focussing rings, are not observed in the water wave case.

Acknowledgements

The authors gratefully acknowledge support from EPSRC under grants EP/J019321/1 (PAM) and EP/J019569/1 (ZW), National Natural Science Foundation of China under grant 11232012 (ZW), and a Royal Society Wolfson award (PAM).

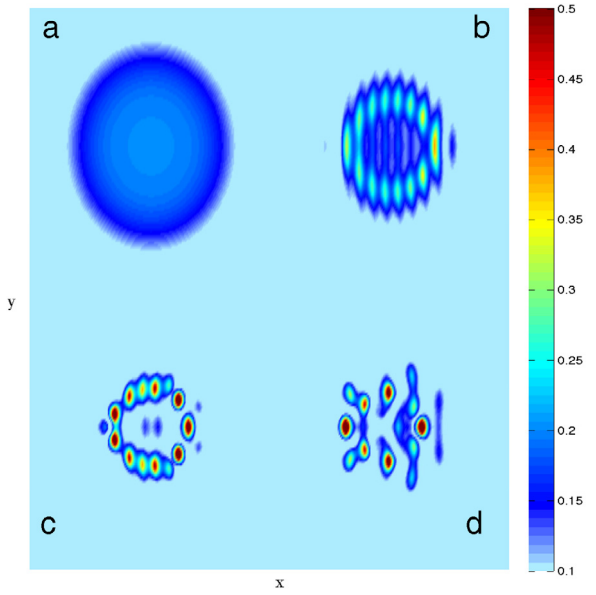

Fig. 12. Viscous evolution of the wave envelope $\mathbb{E}$ extracted from (1)–(2) with an initial super-Gaussian profile as in (9)–(10). The parameters are as in Fig. 2. The images are from left to right taken at (a) $t = 0$ (b) $t = 180$ (c) $t = 240$ (d) $t = 300$. The NLS collapse time is ≈ 306. The initial $\mathcal{H} = 238.7$ and at $t = 300$, $\mathcal{H} = 113.5$.

References

[1] D.J. Benney, A.C. Newell, Propagation of nonlinear wave envelopes, J. Math. Phys. 46 (1967) 133–139.
[2] M.J. Ablowitz, H. Segur, On the evolution of packets of water waves, J. Fluid Mech. 92 (1979) 691–715. http://dx.doi.org/10.1017/S0022112079000835.
[3] B. Kim, T.R. Akylas, On gravity–capillary lumps, J. Fluid Mech. 540 (2005) 337–351. http://dx.doi.org/10.1017/S0022112005005823.
[4] V.E. Zakharov, Collapse of langmuir waves, Sov. Phys. IETP 35 (5) (1972) 908–914.
[5] X. Zhang, Capillary–gravity and capillary waves generated in a wind wave tank: observations and theory, J. Fluid Mech. 289 (1995) 51–82.
[6] E.I. Părău, J.-M. Vanden-Broeck, M.J. Cooker, Nonlinear three-dimensional gravity–capillary solitary waves, J. Fluid Mech. 536 (2005) 99–105. http://dx.doi.org/10.1017/S0022112005005136.
[7] V. Manakov, V.E. Zakharov, L.A. Bordag, A.R. Its, V.B. Matveev, Two dimensional solitons of the kadomtsev-petviashvili equation and their interaction, Phys. Lett. 63 (1977) 205–206.
[8] P.A. Milewski, Three-dimensional localized gravity–capillary waves, Commun. Math. Sci. 3 (2005) 89–99.
[9] R.Y. Chiao, E. Garmire, C.H. Townes, Self-trapping of optical beams, Phys. Rev. Lett. 13 (1964) 479–482. http://dx.doi.org/10.1103/PhysRevLett.13.479.
[10] Z. Wang, P.A. Milewski, Dynamics of gravity–capillary solitary waves in deep water, J. Fluid Mech. 480 (2012) 480–501. http://dx.doi.org/10.1017/jfm.2012.320.
[11] B. Akers, P.A. Milewski, A model equation for wavepacket solitary waves arising from capillary–gravity flows, Stud. Appl. Math. 122 (2009) 249–274.
[12] J. Diorio, Y. Cho, J.H. Duncan, T.R. Akylas, Gravity–capillary lumps generated by a moving pressure source, Phys. Rev. Lett. 103 (2009) 214502. http://dx.doi.org/10.1103/PhysRevLett.103.214502.
[13] K. Berger, P.A. Milewski, The generation and evolution of lump solitary waves in surface-tension-dominated flows, SIAM J. Appl. Math. 61 (2000) 731–750.
[14] E. Falcon, C. Laroche, S. Fauve, Observation of gravity–capillary wave turbulence, Phys. Rev. Lett. 98 (2007) 094503. http://dx.doi.org/10.1103/PhysRevLett.98.094503.
[15] B. Kibler, J. Fatome, C. Finot, G. Millot, F. Dias, G. Genty, N. Akhmediev, J. Dudley, The peregrine soliton in nonlinear fibre optics, Nat. Phys. 6 (2010) 790–795. http://dx.doi.org/10.1038/nphys1740.
[16] J. Fatome, C. Finot, G. Millot, A. Armaroli, S. Trillo, Observation of optical undular bores in multiple four-wave mixing, Phys. Rev. X 4 (2) (2014) 021022.
[17] K.D. Moll, A.L. Gaeta, G. Fibich, Self-similar optical wave collapse: Observation of the townes profile, Phys. Rev. Lett. 90 (2003) 203902. http://dx.doi.org/10.1103/PhysRevLett.90.203902.
[18] G. Fibich, N. Gavish, X.-P. Wang, New singular solutions of the nonlinear schrödinger equation, Physica D 211 (2005) 193–220. http://dx.doi.org/10.1016/j.physd.2005.08.007.
[19] T.D. Grow, A.A. Ishaava, L.T. Vuong, A.L. Gaeta, N. Gavish, G. Fibich, Collapse dynamics of super-gaussian beams, Opt. Express 14 (12) (2006) 5468–5475. http://dx.doi.org/10.1364/OE.14.005468.
[20] R.W. Boyd, S.G. Lukishova, Y.R. Shen, Self-focusing: Past and present, Topics Appl. Phys., Vol. 114.

[21] P.M. Bennett, A. Aceves, Numerical integration of Maxwell's full-vector equations in nonlinear focusing media, Physica D 184 (1–4) (2003) 352–375. http://dx.doi.org/10.1016/S0167-2789(03)00240-9.
[22] F. Dias, A.I. Dyachenko, V.E. Zakharov, Theory of weakly damped free-surface flows: A new formulation based on potential flow solutions, Phys. Lett. A 372 (2008) 1297–1302. http://dx.doi.org/10.1016/j.physleta.2007.09.027.
[23] G. Fibich, Self-focusing in the damped nonlinear schrödinger equation, SIAM J. Appl. Math. 65 (2001) 1680–1705. http://dx.doi.org/10.1137/S0036139999362609.
[24] M. Ohta, G. Todorova, Remarks on global existence and blowup for damped nonlinear schrödinger equation, Discrete Contin. Dyn. Syst. 23 (2009) 1313–1325.
[25] V.M. Pérez-García, M.A. Porras, L. Vázquez, The nonlinear schrödinger equation with dissipation and the moment method, Phys. Lett. A 202 (1995) 176–182. http://dx.doi.org/10.1016/0375-9601(95)00263-3.
[26] N. Huang, Z. Shen, S. Long, A new view of nonlinear water waves: the hilbert spectrum, Annu. Rev. Fluid Mech. 31 (1999) 417–475. http://dx.doi.org/10.1146/annurev.fluid.31.1.417.